Journal of Energy Chemistry 26 (2017) 390–397

Contents lists available at ScienceDirect

Journal of Energy Chemistry

journal homepage: www.elsevier.com/locate/jechem

http://www.journals.elsevier.com/journal-of-energy-chemistry/

Enhanced hydrogen production activity over BiO_X–TiO_2 under solar irradiation: Improved charge transfer through bismuth oxide clusters

Police Anil Kumar Reddy [a,b], Chennaiahgari Manvitha [c], Pullagurala Venkata Laxma Reddy [d], Ki-Hyun Kim [a,*], Valluri Durga Kumari [b,*]

[a] Department of Civil & Environmental Engineering, Hanyang University, 222, WangsimniRo, Seoul 133-791, Republic of Korea
[b] Inorganic and Physical Chemistry Division, Indian Institute of Chemical Technology, Hyderabad 500 607, India
[c] Sarojini Naidu Vanitha Mahavidyala, Osmania University, Hyderabad 500 001, India
[d] Program in Environmental Science and Engineering, University of Texas El Paso, El Paso, Texas 799038, USA

ARTICLE INFO

Article history:
Received 14 September 2016
Revised 24 November 2016
Accepted 19 December 2016
Available online 29 December 2016

Keywords:
Bismuth
TiO_2 nanotubes
Visible photocatalysis
Water splitting
Hydrogen

ABSTRACT

A series of titania nanoparticles and nanotubes deposited with various quantities of bismuth (Bi) were prepared via sol-gel and hydrothermal methods, respectively. They were then characterized using X-ray diffraction spectroscopy (XRD), X-ray photo electron spectroscopy (XPS), UV–Vis diffused reflectance spectra (DRS), photoluminescence spectra (PLS), transmission electron microscopy (TEM), energy dispersive analysis of X-rays (EDAX), and BET surface analysis. These catalysts were employed for the photocatalytic production of hydrogen from a mixture of pure water and glycerol under solar light irradiation. The presence of the $Bi^{(3+x)+}$ species was found to play a vital role in enhancing activity while minimizing electron hole recombination (relative to bare TiO_2). The nanotubes exhibited better activity than the nanoparticles of Bi-deposited TiO_2, showing the significance of the morphology; however, photocatalytic activity is predominantly dependent on the deposition of bismuth. The activity increased by approximately an order of magnitude at the optimum concentration of Bi deposited over TiO_2 (2 wt%). The presence of the $Bi^{(3+x)+}$ species played a vital role in minimizing electron hole recombination, resulting in higher activity compared to bare TiO_2.

1. Introduction

Over the last few years, intensive research has been undertaken in the field of photocatalysis to develop heterogeneous photocatalysts for energy and environmental applications [1–3]. The photocatalytic production of hydrogen mediated via a semiconductor is a feasible and renewable alternate approach to the conventional methods of production from fossil fuels. Among various semiconductor photocatalysts, TiO_2 has been the preferable option, because its band positions are well suited for both the oxidation and reduction of water. However, due to intrinsic large band gap characteristics, charge carriers in TiO_2 can only be excited under UV light irradiation. Enormous efforts have been made to overcome this limitation and to extend the absorption of TiO_2 into the visible region while reducing the recombination of charge carriers.

Non-metal doping (N, S, C, F, and Cl) is considered an effective strategy to improve the visible absorption of TiO_2 into the visible region [4–6]. In general, anion doping can efficiently enhance visible light absorption, as it decreases the band gap of TiO_2 by creating impurity energy levels. TiO_2 doping with some metals (e.g., V, Fe, Co, and Cu) has also been reported, wherein the metal ion dopants not only improved the visible absorption of TiO_2 but also reduced the recombination of the charge carrier by acting as electron sinks [7–10]. Recently, several types of Bi-based photocatalysts were synthesized; they were seen to exhibit enhanced activities under visible and solar light irradiation [11–13]. Doping can result in extension of the absorption spectrum to include the visible range and improvements in the transportation of charge carriers via decreases incharge carrier recombination [14–16]. In addition, nano-structured photocatalysts are generally found to exhibit enhanced activity when compared to nanoparticles in water splitting reactions [17]. Note that nano-structures with tubular morphology have unique characteristics such as large surface area, extended band potentials, and delocalization of electrons along the uni-directional axis that are essential for improving photocatalytic efficiency. Previously, Bi-doped TiO_2 nanoparticles were demonstrated to exhibit improved photocatalytic activity in the degradation of isoproturon under solar light irradiation [18,19]. This

* Corresponding authors.
E-mail addresses: kkim61@haynyang.ac.kr, kkim61@nate.com (K.-H. Kim), durgavalluri@rediffmail.com (V.D. Kumari).

http://dx.doi.org/10.1016/j.jechem.2016.12.007
2095-4956/

encouraged us to prepare Bi-deposited TiO_2 nanotubes to extend the range of absorbable visible light and to improve charge mobility through morphology modification. In this work, we attempt to provide a better understanding of the structure of Bi-TiO_2 photocatalysts through a comparative analysis of various characterization techniques. Based on this work, we also present a plausible scheme for hydrogen production over bismuth deposited TiO_2.

2. Experimental

2.1. Preparation of TiO_2 nanoparticles and nanotubes

Bi-deposited TiO_2 nanoparticles (BT) were prepared via a combination of sol–gel and a co-precipitation method. Acetic acid (1.5 mL) was dissolved in 18 mL ethanol and stirred vigorously. To this solution, 2 mL of $Ti(OC_3H_7)_4$ dissolved in 18 mL ethanol was added dropwise and stirred vigorously for 1 h. A calculated amount (depending on the wt% bismuth) of $Bi(NO_3)_3{\cdot}5H_2O$ dissolved in 5 mL 4 M HNO_3 was added to the above mixture of solution and stirred for another 2 h. The resultant solution was neutralized with aqueous ammonia and stirred vigorously. The solid product was separated, washed with deionized water, dried at 60 °C in the oven for 12 h, and then calcined at 400 °C for 2 h. An undoped TiO_2 (bare TiO_2) sample was also prepared using the same procedure, although without the addition of bismuth nitrate solution. A series of catalysts were prepared by adding varying quantities of Bi (0, 1.0, 2.0, 3.0, and 5.0 wt%) to TiO_2, and these were labeled BT0, BT1, BT2, BT3, and BT5, respectively.

Bismuth-deposited TiO_2 nanotubes (BTNT) were synthesized via a hydrothermal method. In a typical synthesis process, BT samples were dispersed in a 160 mL NaOH aqueous solution (10 M) contained in a 200 mL Teflon container. These samples were placed in a stainless steel autoclave and heated at 130 °C for 36 h. The precipitate was then washed twice with deionized water and treated with 0.1 M HCl. The suspension was again washed with deionized water, dried at 60 °C for 12 h, and calcined at 350 °C for 2 h. The Bi-deposited TiO_2 nanotubes are labelled BTNT1, BTNT2, BTNT3, and BTNT5.

The catalysts prepared were characterized using XRD, BET, XPS, EDAX, TEM, UV–Vis DRS, and photoluminescence spectroscopy. Powder X-ray diffraction patterns were recorded on a “Rigaku” diffractometer using Cu $K\alpha$ radiation (0.1540 nm). The surface area of the catalysts was measured using an “Autosorb 1C Quantachrome” physical adsorption apparatus. UV–Vis DRS measurements were recorded in a wavelength range of 200–800 nm using a GBC UV–Visible “Cintra 10e spectrometer” with an integration sphere diffuse reflectance attachment. XPS spectra were recorded with a “KRATOS AXIS 165” apparatus equipped with Mg $K\alpha$ radiation (1253.6 eV) at 75 W using a Mg $K\alpha$ anode and a hemispherical analyzer, connected to a five-channel detector. The C 1*s* line at 284.6 eV was used as an internal standard for the correction of binding energies. Elemental analysis was carried out using the “Link, ISIS-300, Oxford” energy-dispersive X-ray spectroscopy (EDAX) detector. TEM and HRTEM studies were performed using a “TECNAI G2” TEM microscope equipped with a slow-scan CCD camera and at an accelerating voltage of 200 kV. The preparation of samples for this analysis involved sonication in ethanol for 10 min and deposition on a copper grid. The photoluminescence spectra were obtained using the “Jasco Spectrofluorometer-FP8000” with an excitation wavelength of 320 nm.

2.2. Photocatalytic experiments

Using the prepared photocatalysts, the photocatalytic production of hydrogen was carried out via water splitting under solar light irradiation. The reaction was performed in a 100 mL tube-like quartz reactor with a round bottom. 5 mg of the catalyst was added to 50 mL of 5% aqueous glycerol solution in a quartz reactor, which was then sealed with an air-tight rubber septum. The reactor was evacuated for 30 min, and the solution was purged with N_2 gas for another 30 min. The reaction was carried out under bright sunlight irradiation (from 10:00 AM to 3:00 PM), with the intensity of the light measured using an LT Lutron LX-101A digital light meter (~ 130,000 Lux). The amount of H_2 gas produced during the course of the reaction was monitored at hourly intervals by taking the gas samples in an airtight syringe. The analysis of the sample was carried out using a gas chromatograph (Shimadzu GC-2014) equipped with a TCD detector and a molecular sieve 5A column with N_2 as a carrier gas.

3. Results and discussion

3.1. Characterization

3.1.1. XRD

The crystal structure of the Bi-deposited TiO_2 samples (BT and BTNT) was examined via XRD in the range of 10°–80° (2θ), as shown in the diffractograms (Fig. 1). According to the diffractograms, all of the Bi- deposited TiO_2 and bare TiO_2 samples produced XRD patterns with the anatase phase of an intense peak

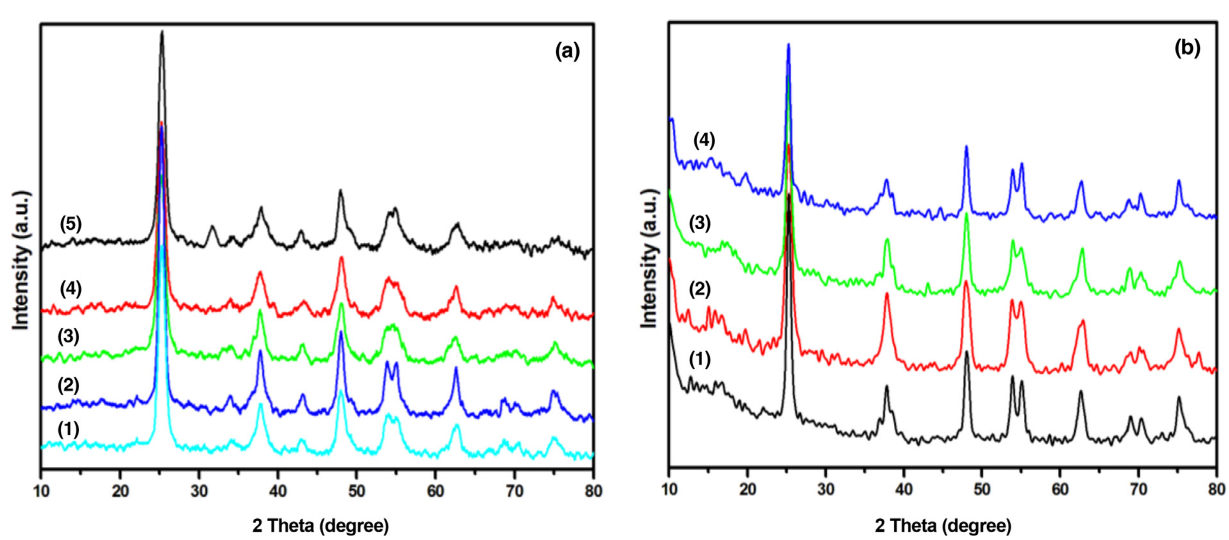

Fig. 1. XRD patterns of different samples. (a): (1) BT0, (2) BT1, (3) BT2, (4) BT3, (5) BT5; (b): (1) BTNT1, (2) BTNT2, (3) BTNT3, (4) BTNT5.

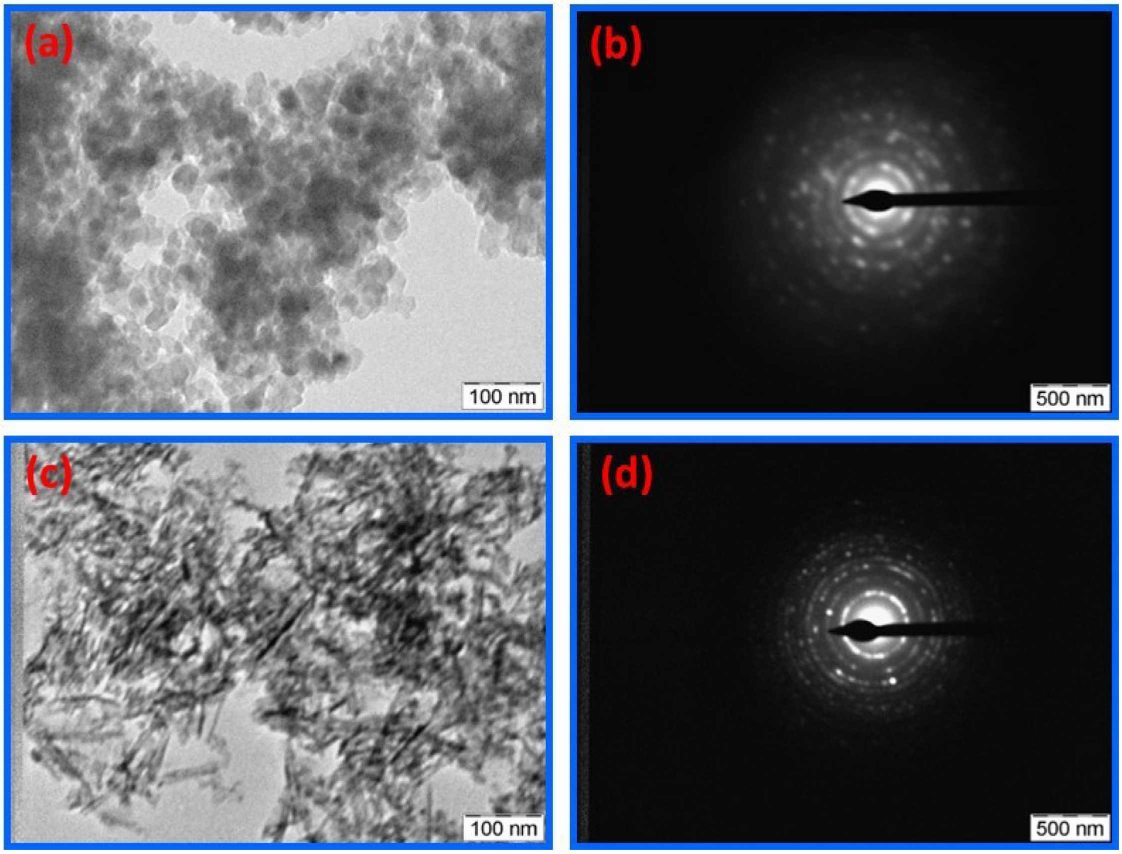

Fig. 2. TEM and SAED patterns of BT2 (a, b) and BTNT2 (c, d).

Table 1. Physical properties of Bi-deposited TiO_2 photocatalysts.

Catalyst	Bi (wt%, expl)	Bi (wt%, EDAX)	BET surface area (m^2/g)
BT0	0	–	112
BT1	1	0.56	108
BT2	2	0.83	102
BT3	3	1.75	99
BT5	5	2.99	83
BTNT1	1	0.55	186
BTNT2	2	0.88	173
BTNT3	3	1.45	168
BTNT5	5	2.04	155

at 25.3° (major peaks at 25.3°, 37.8°, 47.9°, and 54.8°; JCPDS No. 21-1272). The addition of up to 3 wt% Bi over TiO_2 did not induce significant changes in the diffractograms of either the BT or BTNT samples. In addition, bismuth deposition did not shift the diffraction angles of the anatase. As such, the bismuth species are not likely to be incorporated into the TiO_2 lattice; they may instead be dispersed as BiO_X on the surface of the TiO_2. The greateratomic size of Bi^{3+}, at 103 pm, which is larger than Ti^{4+} at 61 pm, may inhibit the replacement of titanium in the crystal lattice of TiO_2 with bismuth [20,21].

This phenomenon is evident as a small peak in the BT5 sample (5 wt% Bi-deposited TiO_2 nanoparticles) with a weak Bi_2O_3 peak at 31.8°, as reported previously [11,18,22]. This observation may reflect the formation of larger bismuth clusters on the surface of TiO_2 with increase in the amounts of bismuth loading. In addition this data confirm that instead of replacing titanium in the TiO_2 crystal lattice, the bismuth species are in the amorphous BiO_X state on the surface of the TiO_2 at low loading quantities. Higher loadings can aid in the formation of Bi_2O_3 crystallites, as a significant change was recognized in the surface area of BT5 sample (Table 1).

In contrast, the BTNT5 sample (5 wt% Bi-deposited TiO_2 nanotubes) did not show the abovementioned peaks, validating that the bismuth oxide species are more evenly dispersed on the nanotubes than on the nanoparticles. The high surface area of nanotubes (Table 1) may facilitate the uniform, thorough dispersion of the bismuth oxide species over their surface (relative to the nanoparticles). In addition, the presence of strong XRD diffraction peaks in the BTNT samples indicates that the prepared Bi-deposited TiO_2 nanotubes (BTNT) were highly crystalline in nature.

3.1.2. TEM

The morphology of the synthesized photocatalysts (BT2 and BTNT2 samples) was observed via TEM analysis (Fig. 2). The TEM image of BT2 nanoparticles in Fig. 2(a) depicts the agglomerated crystallites of TiO_2 with crystallite sizes in the range of 15–20 nm. The selected area electron diffraction pattern of BT2 shown in Fig. 2(c) demonstrates their polycrystalline nature, while the circular rings originating from the planes of (101), (004), (211), and (200) correspond to tetragonal crystallites of anatase TiO_2. The TEM image of BTNT2 shown in Fig. 2(b) confirms the nanotube morphology of the prepared sample; the addition of bismuth did not restrict the formation of nanotubes. This image also shows tubular structures with lengths and diameters of approximately 100 and 10 nm, respectively. Fig. 2(d) presents SAED patterns of the BTNT2 sample; the diffraction patterns with bright spots correspond to the planes of (101), (004), (211), and (200) of anatase TiO_2 crystallites. The bright diffraction patterns of the BTNT2 sample further confirm its higher crystalline nature relative to the BT2 sample.

3.1.3. XPS

To investigate the chemical states of the possible dopants incorporated into TiO_2, the binding energies of Ti 2*p*, O 1*s*, and Bi 4*f*

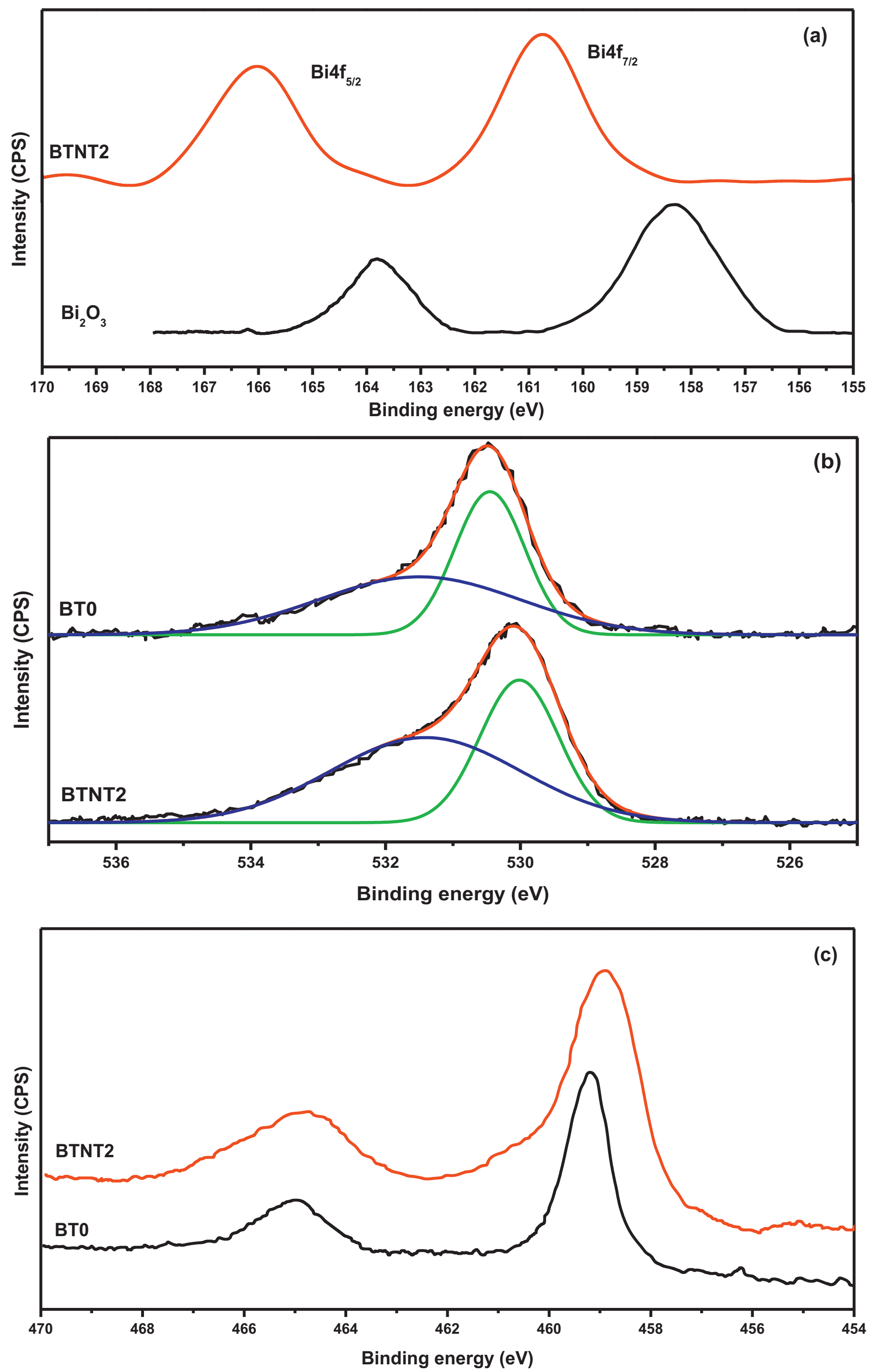

Fig. 3. XPS of (a) Bi 4*f*, (b) O 1*s*, and (c) Ti 2*p*.

were studied by recording the XPS spectra. The results are shown in Fig. 3.

Two peaks for Bi $4f_{7/2}$ and Bi $4f_{5/2}$ at 158.3 and 163.8 eV, respectively, were observed in the XPS spectra of pure Bi_2O_3. In contrast, 2 wt% Bi-deposited TiO_2 nanotubes (BTNT2) show the presence of two peaks (Bi $4f_{7/2}$ and Bi $4f_{5/2}$) at 160.8 and 166.0 eV, respectively, which are higher than those of the pure Bi_2O_3 (Fig. 3a). The positive shift towards a higher binding energy indicates that the Bi^{3+} centers are partially oxidized to $Bi^{(3+x)+}$ [23]. This enhancement of binding energy may be due to the formation of Bi–O–Ti bonds in the Bi-deposited TiO_2 [24]. Interestingly, the BTNT2 sample did not exhibit peaks corresponding to Bi–O–Bi (located at approximately 162.5 and 157.3 eV of pure Bi_2O_3). The bismuth species were well dispersed, enabling efficient interaction with the TiO_2 support. The partial substitution of Ti^{4+} with $Bi^{(3+x)+}$ will create oxygen vacancies in order to make a charge neutrality in the Bi-deposited TiO_2 [25]. Thus, the presence of $Bi^{(3+x)+}$ is relevant to vacant oxygen sites that are produced in the structure of the material. The presence of $Bi^{(3+x)+}/Bi^{3+}$ species in the catalyst favors the trapping of electrons to facilitate the separation of electron-hole pairs in the photocatalytic process.

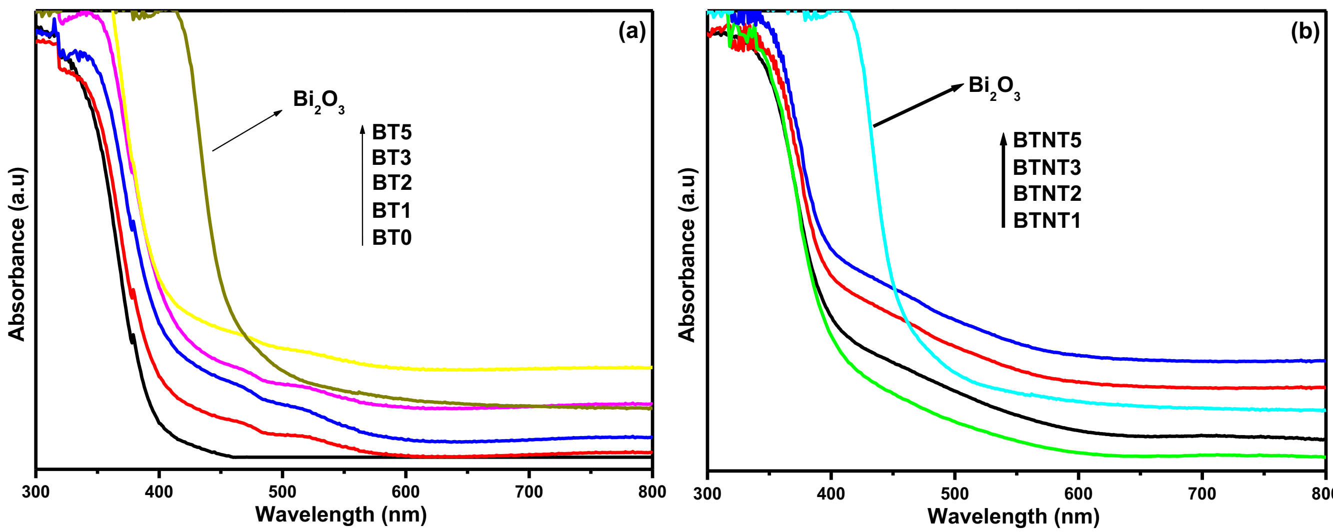

Fig. 4. UV–Vis DRS of Bi-deposited TiO_2: (a) BT and (b) BTNT catalysts.

The O 1*s* spectra shown in Fig. 3(b) are wide and asymmetric, indicating that there are at least two types of oxygen chemical states. The samples exhibit binding energies ranging from 528 to 534 eV. As shown in Fig. 3(b), the contribution for O 1*s* may be accounted for in two aspects: the intense peak, located at approximately 530 eV, is assigned to crystal lattice oxygen (O_L), while the broad peak located at 532 eV is ascribed to hydroxyl oxygen (O_H) [26,27]. The relative intensity of hydroxyl oxygen increased with Bi deposition. Explanations for this phenomenon may be sought from the lower valence and larger ion radius of Bi^{3+} compared to that of Ti^{4+}. As such, the formation of defects should have led to the higher hydroxyl number on the surface of Bi-deposited TiO_2.

The Ti 2*p* spectra of bare TiO_2 (BT0) and BTNT2 are shown in Fig. 3(c). The BT0 sample exhibits two sharp peaks for Ti^{4+}, one at 458.6 eV for Ti $2p_{3/2}$ and the other at 464.8 eV for Ti $2p_{1/2}$. The peak for Ti 2*p* became wider for 2 wt% Bi-deposited TiO_2 (BTNT2). This broad peak may be ascribable to one of two factors: (i) the formation of Ti–O–Bi shifts the electron density toward the Ti atom, resulting in a shift toward lower energy [18,23], or (ii) an increasing Bi content leads to the formation of more defects. This induced the formation of surface hydroxyl groups on the TiO_2 surface; thus the amount of Ti–OH also increased, leading to a shift towards higher energy.

3.1.4. UV–Vis DRS

Light absorption properties of the synthesized samples (BT and BTNT catalysts) were studied via UV–Vis DR spectroscopy (Fig. 4). The bare TiO_2 exhibits an intense absorption band at approximately 380 nm in the ultraviolet region. In contrast, Bi deposition led to an increase of absorption in the visible region. The extended absorption of the Bi-modified TiO_2 samples in the visible region with increased Bi loading led to the reduction in the band gap of the Bi–TiO_2 catalyst relative to bare TiO_2. This result indicates that Bi deposition can enlarge the wavelength response range, and the effect of Bi deposition on visible-light response should be ascribable to the formation of Ti–O–Bi in titania nanotubes. The absorption increase in the visible range might be explained by the induction of the narrower band gap via the energy state of Bi^{3+} 6*s* lone pairs lying above the valence band of sole TiO_2 [28,29].

The theory predicting a shift in the absorption edge of TiO_2 via bismuth deposition was explained previously. Wei et al. [30] suggested that the bismuth doping should lead to a change in the electronic environment surrounding the surface titanium atoms. They systematically studied the interaction of bismuth oxide clusters with a TiO_2 surface and found that the Bi–O distances in the surface nanoclusters were shorter because of the lower coordination of Bi in the nanoclusters compared to the bulk of Bi_2O_3. They also investigated the surface Ti atoms, which were bound to the BiO_X nanoclusters and were pulled out of the surface layer through the interaction with oxygen. This displacement caused lengthening of the subsurface Ti–O bonds. These cumulative effects caused by a lower coordination of Bi and increased Ti–O bond length led to changes in the geometry and polarity of the Ti and Bi atoms. As such, the possibility of defects formation increased systematically; this may be the reason for the improved visible absorption of the Bi deposited TiO_2 photocatalysts [30].

3.1.5. Photoluminescence spectra

Photocatalytic activity depends on the efficiency of the photogenerated electron–hole separation and the transfer of charge carriers from the inner regions to the outer surfaces. When the photoinduced charge carriers recombine, they emit photoluminescence proportional to the recombination rate of the charge carrier. Hence, photo luminescence (PL) spectra are useful in determining the efficiency of several processes, including charge carrier trapping, migration, and transfer, and in understanding the nature of electron–hole pairs in semiconductor particles.

To address the effects of Bismuth deposition on electron–hole separation, photoluminescence spectroscopy (PL) was employed through characterization of the recombination probability of BT0 (bare TiO_2), BT2, and BTNT2 photocatalysts. The PL spectra of these photocatalysts are displayed in Fig. 5 in a wavelength range of 350–550 nm. The emission peak at 390–410 nm is a result of phonon-assisted indirect transition from the edge (*M*) to the center (Γ) of the Brillouin zone [31]. The emission peak at 429 nm is assigned to self-trapped excitons localized on TiO_6 octahedra [32]. After photoexcitation at 320 nm, the electrons in the conduction band move through the ionic lattice, interact with the lattice ions, and then localize on a lattice site. The localized electron captures a hole and generates self-trapped excitons [33]. The emission peaks at 457 nm and 537 nm are associated with oxygen-related defect states [32]. The emission peak at 491 nm is ascribed to charge transfer transition from Ti^{3+} to ${TiO_6}^{2-}$ octahedra [34,35].

It is important to note that the luminescence intensities of the BT2 and BTNT2 photocatalysts are lower than that of pristine TiO_2, confirming the higher probability of electron–hole recombination

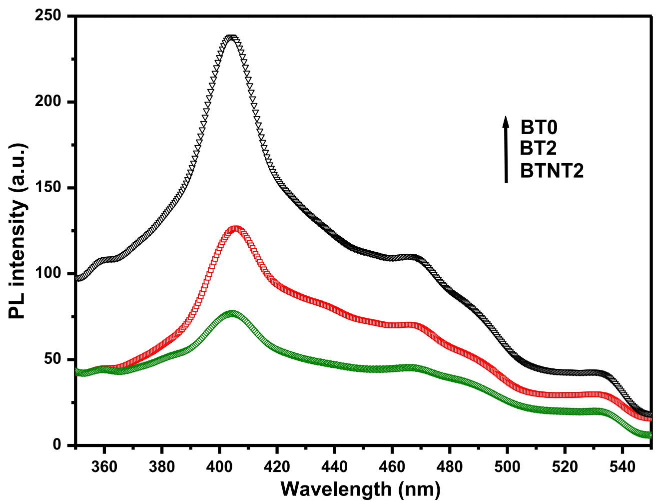

Fig. 5. Photoluminescence spectra of BT0, BT2, and BTNT2 catalysts.

in the latter. This may be ascribed to the fact that Bi species reduced the number of trap states on the surface of the TiO_2, thus improving the separation of photogenerated charge carriers. The decreased recombination of photogenerated charges will provide more opportunities for photo-induced charge carriers to participate in the photocatalytic reactions on the semiconductor surface. In addition, BT2 exhibits peaks with higher intensity when compared to BTNT2, possibly because the nanotube morphology (BTNT2) accelerates the transfer of excited charge carriers to the surface when compared to the nanoparticle morphology (BT2). This phenomenon may be the reason for the higher activity of the BTNT2 catalysts over that of the BT2 catalysts for hydrogen production (discussed in the "photocatalytic activity" section). Hence, PL studies confirm that Bi deposition may have slowed the radiative recombination process of photogenerated electrons and holes in TiO_2, while the nanotube morphology improved the charge carrier mobility in Bi-deposited TiO_2. These combined effects are beneficial to the improved catalytic efficiency of bismuth-deposited TiO_2 catalysts.

3.2. Photocatalytic activity evaluation

The photocatalytic performances of the as-prepared samples were evaluated via photocatalytic H_2 evolution rates in 5% glycerol aqueous solution under solar light irradiation conditions. Fig. 6(a,b) shows the photocatalytic activities of various bismuth-deposited TiO_2 catalysts (BT and BTNT) with respect to hydrogen production as a function of time. All samples exhibit photocatalytic activities for hydrogen production. The optimum hydrogen production of 2345 μmol/g/h was observed in BTNT2 after 5 h irradiation; this rate is approximately 20 times that of the bare TiO_2 (105 μmol/g/h).

Explanations for the enhanced photocatalytic activity of Bi-deposited TiO_2 relative to bare TiO_2 may be sought for by the following factors: (i) the impurity levels formed by the bismuth species (hybridization of Bi 6*s* and O 2*p*) extended the visible absorption by decreasing the band gap of TiO_2, as evidenced from UV–Vis DRS [11] and (ii) an increase in the lifetime of the charge carriers. It is known that the 4*f* level of the bismuth ion can trap the photo-excited electrons, leading to enhanced lifetime of the charge carriers [30]. However, it was observed that photocatalytic activity increased with increased bismuth loading, although this effect decreased with further loading. According to the aforementioned characterizations, such reduction at higher bismuth loadings can be attributed to the formation of bismuth oxide clusters (observed via XRD) that can act as recombination centers for electrons and holes.

It can be clearly observed that the Bi-deposited TiO_2 nanotubes (BTNT samples in Fig. 6b) exhibited a higher photocatalytic activity than the Bi-deposited TiO_2 nanoparticles (BT samples in Fig. 6a). The higher activity of the BTNT catalysts compared to the BT catalysts might be due to differences in the morphologies. The majority of the generated charge carriers in BT nanoparticles undergo fast recombination, and only a fraction are utilized for H_2 generation (as evidence by PL spectra). However, a significant improvement in H_2 evolution was observed with BTNT nanotubes as photocatalysts due to the delocalization of electrons along the axis of the nanotube. The highest H_2 production achieved by BTNT2 photocatalyst should reflect a combined effect of several factors such as: (1) quantum confinement by photogenerated electrons (due to a favourable structure of TiO_2 nanotube for the delocalization of electrons along the uni-directional axis), (2) the efficient separation of electrons, and (3) proton reductions at $Bi^{(3+x)+}$ sites. Thus the highly efficient photocatalytic activity of BTNT2 is ascribed to the following factors: (i) efficient solar light absorption, (ii) fast charge carrier transfer due to nanotube morphology, (iii) efficient separation and fast reduction of protons to H_2 by $Bi^{(3+x)+}$ centers, (iv) the effective adsorption of reactants involved in charge carrier utilization and the desorption of products.

To evaluate the sustainability of the photocatalysts, the photocatalytic activity of the BTNT2 sample was studied for extended periods of time (up to 20 h), as shown in Fig. 6(c). It can be observed from the data that the activity increased linearly up to 5 h, and increased slowly after 10 h of reaction. The decrease in the rate of hydrogen production with time (after 10 h) may be due to the pressure developed by the produced hydrogen during the course of the reaction. This is also evidenced by the color change of the solution from light yellow to a thick black color (not shown) during the track of the reaction. After several hours, the volume of the reactor became insufficient to accommodate the amount of H_2 generated from the water splitting. Thus, with the increased partial pressure of H_2 in the reactor, further dissolution of H_2 took place in the solution phase. As the number of active sites on the surface of the photocatalysts was reduced, the rate of H_2 evolution was also retarded [36]. To confirm this, the recycling activity of the BTNT2 catalysts was assessed. When the produced gases were evacuated and purged with N_2 at five-hour intervals, the activity of the catalyst was retained and for up to 25 h (Fig. 6d). This confirms that the catalyst is sustainable for longer periods of time, provided that the evolved gasses are removed or evacuated at regular intervals.

3.3. Structure activity correlation

The photocatalytic mechanism of Bi–TiO_2 catalysts and the role of Bi in the system are shown in Fig. 7. In Bi-deposited TiO_2 catalysts, bismuth deposition created the $Bi^{(3+x)+}$ species and impurity energy levels both above and below the valance and conduction bands of TiO_2, which resulted in a reduction in band-gap energy, as shown in Fig. 7. Under photo irradiation, Bi–TiO_2 can produce electron-hole pairs; and the electrons are expected to be trapped by the higher oxidation state of the bismuth ($Bi^{(3+x)+}$), which is converted to the Bi^{3+} species; this aids in the separation of the electron-hole pairs. The decrease in the recombination of charge carriers is consistent with the obtained photoluminescence spectra results. After electron-hole separation, the excited electrons are trapped by the $Bi^{(3+x)+}$ species and can be transferred to the protons in the reaction media, thus leading to the production of hydrogen. In light of XRD, XPS, and photoluminescence spectra, it can be concluded that the $Bi^{(3+x)+}$ works efficiently as a charge separation center and is responsible for higher activity. It is clear that at intermediate loading of Bi–TiO_2, Bi is present as $Bi^{(3+x)+}$, which

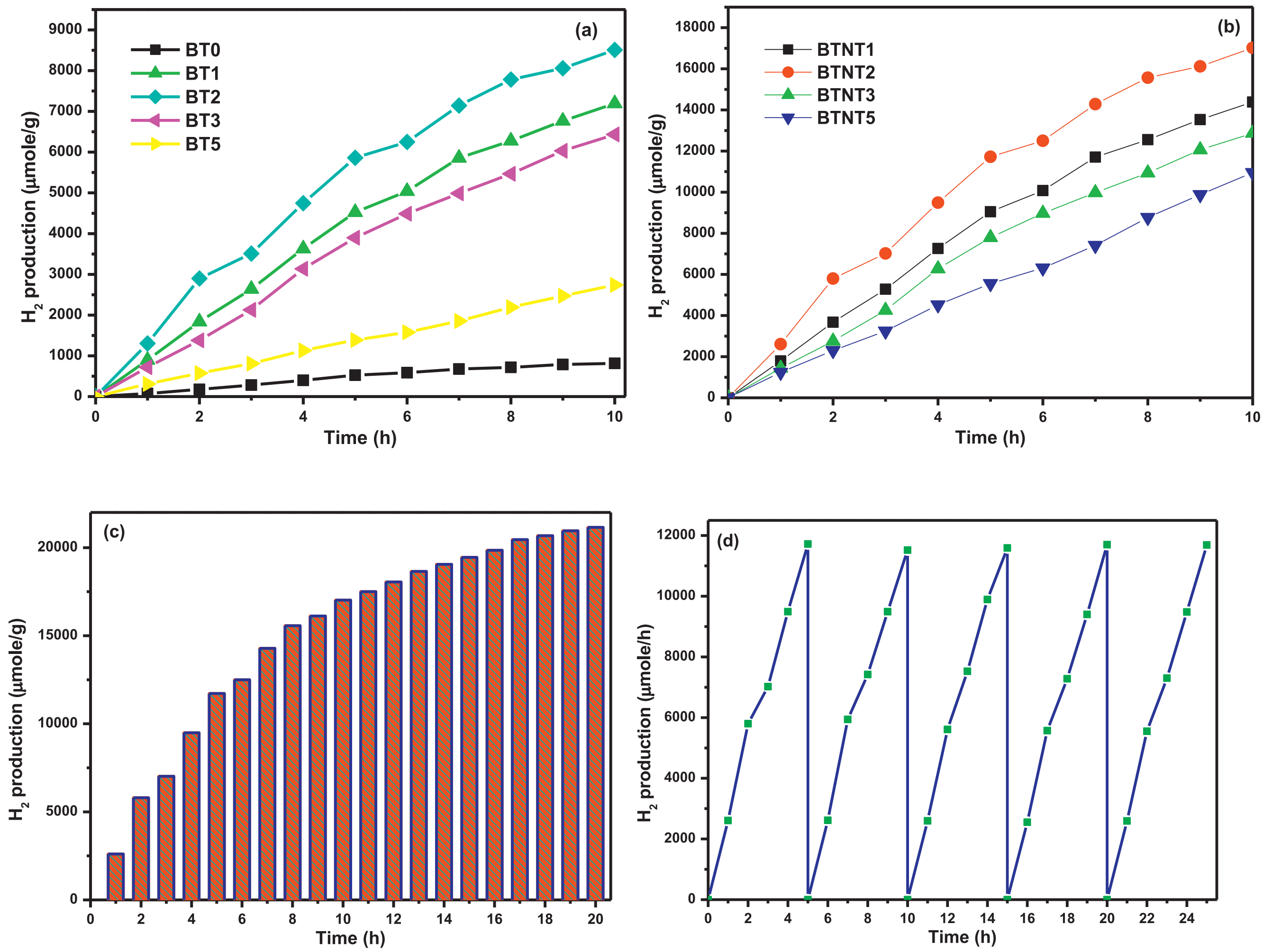

Fig. 6. Photocatalytic activity of Bi-(wt%)-deposited TiO_2 for hydrogen production under solar light irradiation with (a) BT and (b) BTNT photocatalysts; (c) Time on stream activity of the BTNT2 catalyst; (d) Recycling studies of the BTNT2 photocatalyst. (For interpretation of the references to color in this figure, the reader is referred to the web version of this article.)

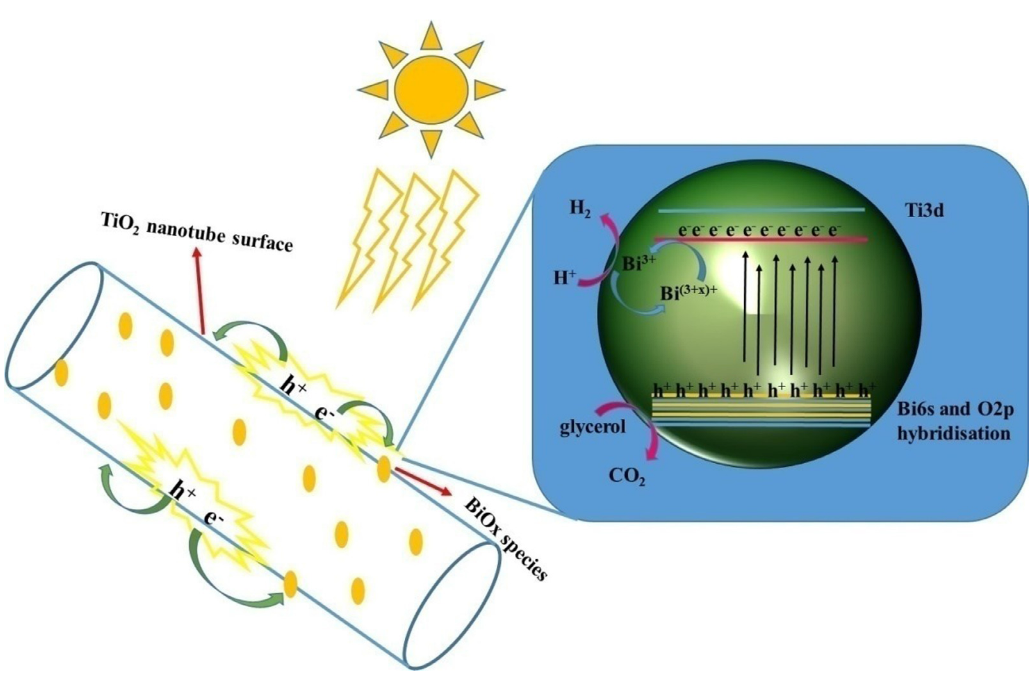

Fig. 7. Plausible photocatalytic excitations in Bi-deposited TiO_2 nanotubes.

functions effectively as a charge separation center, playing a major role in reducing the recombination of electron-hole pairs.

4. Conclusions

The present study describes the preparation of Bi-deposited TiO_2 photocatalysts and discusses the role of highly-dispersed BiO_X species on the photo-catalytic production of hydrogen from glycerol aqueous solution under solar light irradiation. 2 wt% Bi-deposited TiO_2 was determined to be an efficient catalyst for the production of hydrogen. It was observed that the morphology of bismuth-deposited TiO_2 has a strong influence on photocatalytic activity. The higher activity of nanotube (BTNT2) catalysts compared to nanoparticle (BT2) catalysts was primarily due to improved charge transfer and charge mobility in the former. This study demonstrates the strong interaction of Bi species with the TiO_2 surface at lower loadings. Thus, the highly interactive Bi species exist in an oxidation state higher than +3. The presence of greatly dispersed $Bi^{(3+x)+}$ species was expected to play a vital role in reducing the recombination of electron and hole pairs. Overall, the high photocatalytic activity of bismuth-deposited TiO_2 photocatalysts was attained via the synergistic effect of stronger absorption in the visible light region and lower electron-hole recombination.

Acknowledgments

The corresponding author (KHK) acknowledges support from a National Research Foundation of Korea (NRF) grant funded by the Ministry of Science, ICT & Future Planning (No. 2016R1E1A1A01940995).

References

[1] A.K.R. Police, S. Basavaraju, D. Valluri, S. Machiraju, Bull. Mater. Sci. 38 (2015) 227–234.
[2] A.K.R. Police, S. Basavaraju, D.K. Valluri, M.V. Shankar, S. Machiraju, J.S. Lee, Chem. Eng. J. 247 (2014) 152–160.
[3] B. Srinivas, B. Shubhamangala, K. Lalitha, P.A.K. Reddy, V.D. Kumari, M. Subrahmanyam, B.R. De, Photochem. Photobiol. 87 (2011) 995–1001.
[4] B. Wang, M.K.H. Leung, X.Y. Lu, S.Y. Chen, Appl. Energy. 112 (2013) 1190–1197.
[5] P.A.K. Reddy, P.V.L. Reddy, V.M. Sharma, B. Srinivas, V.D. Kumari, M. Subrahmanyam, J. Water. Resour. Prot. 2 (2010) 235–244.
[6] X.K. Wang, C. Wang, W.Q. Jiang, W.L. Guo, J.G. Wang, Chem. Eng. J. 189-190 (2012) 288–294.
[7] A.K. Agegnehu, C.J. Pan, M.C. Tsai, J. Rick, W.N. Su, J.F. Lee, B.J. Hwang, Int. J. Hydrog. Energy 41 (2016) 6752–6762.
[8] G. Sadanandam, K. Lalitha, V.D. Kumari, M.V. Shankar, M. Subrahmanyam, Int. J. Hydrog. Energy 38 (2013) 9655–9664.
[9] D.P. Kumar, N.L. Reddy, B. Srinivas, V. Durgakumari, V. Roddatis, O. Bondarchuk, M. Karthik, Y. Ikuma, M.V. Shankar, Sol. Energy Mater. Sol. Cells 146 (2016) 63–71.
[10] J.K. Reddy, K. Lalitha, P.V.L. Reddy, G. Sadanandam, M. Subrahmanyam, V.D. Kumari, Catal. Lett. 144 (2014) 340–346.
[11] W. Wang, D. Zhu, Z. Shen, J. Peng, J. Luo, X. Liu, Ind. Eng. Chem. Res. 55 (2016) 6373–6383.
[12] A.K.R. Police, S. Basavaraju, D.K. Valluri, S. Machiraju, J. Mater. Sci. Technol. 29 (2013) 639–646.
[13] M.K. Kumar, K. Bhavani, B. Srinivas, S.N. Kumar, M. Sudhakar, G. Naresh, A. Venugopal, Appl. Catal. A. 515 (2016) 91–100.
[14] P.V.L. Reddy, K.H. Kim, Y.H. Kim, Asian. J. Atmospheric Environ. 5 (2011) 181–188.
[15] P.V.L. Reddy, K.H. Kim, J. Hazard. Mater. 285 (2015) 325–335.
[16] P.A.K. Reddy, P.V.L. Reddy, E. Kwon, K.H. Kim, T. Akter, S. Kalagara, Environ. Int. 91 (2016) 94–103.
[17] H. Tong, S. Ouyang, Y. Bi, N. Umezawa, M. Oshikiri, J. Ye, Adv. Mater. 24 (2012) 229–251.
[18] P.A.K. Reddy, B. Srinivas, P. Kala, V.D. Kumari, M. Subrahmanyam, Mater. Res. Bull. 46 (2011) 1766–1771.
[19] P.A.K. Reddy, B. Srinivas, V. Durgakumari, M. Subrahmanyam, Toxicol. Environ. Chem. 94 (2012) 512–524.
[20] J. Yang, X. Wang, J. Dai, J. Li, Ind. Eng. Chem. Res. 53 (2014) 12575–12586.
[21] Z. Bian, J. Zhu, S. Wang, Y. Cao, X. Qian, H. Li, J. Phys. Chem. C. 112 (2008) 6258–6262.
[22] Q.M. Kang, B.L. Yuan, J.G. Xu, M.L Fu, Catal. Lett. 141 (2011) 1371–1377.
[23] S. Sajjad, S.A.K. Leghari, F. Chen, J. Zhang, Chem. Eur. J. 16 (2010) 13795–13804.
[24] Y. Yang, X. Wang, X. Yang, J. Li, X. Zhang, J. Zhao, Electrochim. Acta. 169 (2015) 227–232.
[25] Y. Wang, Y. Wang, Y. Meng, H. Ding, Y. Shan, X. Zhao, X. Tang, J. Phys. Chem. C. 112 (2008) 6620–6626.
[26] M.V. Kuznetsov, J.F. Zhuravlev, M.F. Gubanov, J. Electron. Spectrosc. Relat. Phenom. 58 (1992) 169–176.
[27] T.L. Barr, J. Phys. Chem. 82 (1978) 1801–1810.
[28] J. Xu, W. Wang, M. Shang, E. Gao, Z. Zhang, J.J. Ren, J. Hazard, Mater. 196 (2011) 426–430.
[29] W.F. Yao, H. Wang, X.H. Xu, X.F. Cheng, J. Huang, S.X. Shang, X.N. Yang, M. Wang, Appl. Catal. A. 243 (2003) 185–190.
[30] W. Wei, Y. Dai, B. Huang, J. Phys. Chem. C. 113 (2009) 5658–5663.
[31] C.H. Ho, M.C Tsai, M.S Wong, Appl. Phys. Lett. 93 (2008) 081904-–081904-3.
[32] Y. Lei, L.D. Zhang, G.W. Meng, G.H. Li, X.Y. Zhang, C.H. Liang, W. Chen, S.X. Wang, Appl. Phys.Lett. 78 (2001) 1125–1127.
[33] J. Preclíková, P. Galář, F. Trojánek, S. Daniš, B. Rezek, I. Gregora, Y. Němcová, P.J. Malý, J. Appl. Phys. 108 (2010) 113502–113508.
[34] J. Liu, J. Li, A. Sedhain, J. Lin, H. Jiang, J. Phys. Chem. C. 112 (2008) 17127–17132.
[35] B. Choudhury, A. Choudhury, J. Lumin. 136 (2013) 339–346.
[36] W.Y. Cheng, T.H. Yu, K.J. Chao, S.Y. Lu, ChemCatChem. 6 (2014) 293–300.